Evolution of PAH Features from Proto- to Planetary Nebulae

R. Szczerba[*], N. Siódmiak[*] and C. Szyszka[†]

[*]*N. Copernicus Astronomical Center, Rabiańska 8, 87-100 Toruń, Poland*
[†]*Toruń Centre for Astronomy of the NCU, Gagarina 11, 87-100 Toruń, Poland*

Abstract. With the aim to investigate the overall evolution of UIR band features with hardening of UV radiation (increase of the star's effective temperature) we have analysed ISO spectra for 32 C-rich stars: 20 proto-planetary nebulae and 12 planetary nebulae with Wolf-Rayet central stars. In this contribution we discuss variations in the peak position of UIR bands among analysed objects, and demonstrate that variations in the "7.7" to 11.3 μm flux ratio are correlated with the effective temperature (probably due to an increase of the ionization state of their carriers).

INTRODUCTION

The presence of unidentified infra-red (UIR) bands around 3.3, 6.2, "7.7", 8.6 and 11.3 μm in many astronomical objects is commonly attributed to polycyclic aromatic hydrocarbon (PAH) molecules which are excited by UV photons (see e.g. Li 2004). After absorption of a single UV photon, energy is redistributed over the molecule and the molecule "cools down" through photon emission in the UIR bands. Possibly, the observed features are due to a complex mixture of ionized and neutral PAH or PAH-related molecules of different sizes. Therefore, the overall appearance of the features (shape, peak position and strength) are determined by the present physical conditions, but also by the formation and evolution of their carriers.

PAHs are thought to be formed in the outflows from C-rich asymptotic giant stars (AGB). However, there is no direct evidence of the presence of these large molecules in circumstellar envelopes of C-rich AGB stars[1]. The most possible explanation of UIRs undetection is the lack of UV photons in surroundings of AGB stars.

Recently, Peeters et al. (2002) and van Diedenhoven et al. (2004) have investigated variations of the UIR features in a large variety of sources including star forming regions, H II regions, Herbig Ae Be stars and galaxies as well as evolutionary advanced stellar objects. However, their sample included only 7 post-AGB objects and 4 planetary nebulae (PNe) with [WR][2] central stars. There-

fore, to investigate variations (and possible evolution) of UIR features in sources with fairly well established physical conditions we have determined parameters of UIR band profiles for the largest available sample of post-AGB objects and [WR] PNe using Infrared Space Observatory (ISO, see Kessler et al. 1996) data.

SAMPLE AND THE UIR FEATURES

We have searched the ISO Data Archive for Short Wavelength Spectrometer (SWS, see de Graauw et al. 1996) data taken with AOT 01 for about 330 post-AGB objects compiled recently by Siódmiak (2005). SWS 01 data are available for 65 sources and UIR bands are present in spectra for 20 of them. The sample of [WR] PNe includes sources which were discussed by Szczerba et al. (2001), however, we excluded 4 objects which do not show UIR bands or have SWS 01 data which do not allow to make a quantitative analysis of their UIR bands.

The ISO Spectral Analysis Package (ISAP 2.1)[3] was used to process and analyze SWS 01 spectra (OLP version 10.1) for all sources from our sample. During data reduction bad data were removed and spectra were rebinned to a constant resolution of 300. Small memory effects were smeared out by direct averaging across up and down scans, but in case of larger memory effects, the up and down scans were averaged separately to investigate changes in the UIR features. The parameters of the UIR band profiles were determined by defining local continua

---

[1] Recently, Boersma et al. (2005) reported the detection of the UIR bands in the Infrared Space Observatory spectrum of the AGB carbon star TU Tau: a binary star which has a blue companion.

[2] Wolf-Rayet planetary nebulae have central stars which are hydrogen poor and lose mass at higher rates than normal central stars, but their chemical composition is similar to that for normal PNe. ISO data have shown that in this group of objects both forms of dust (C-

rich: responsible for UIR bands and O-rich: responsible for crystalline silicate features) are present (Waters et al. 1998, Cohen et al. 1999).

[3] The ISO Spectral Analysis Package (ISAP) is a joint development by the LWS and SWS Instrument Teams and Data Centers. Contributing institutes are CESR, IAS, IPAC, MPE, RAL and SRON.
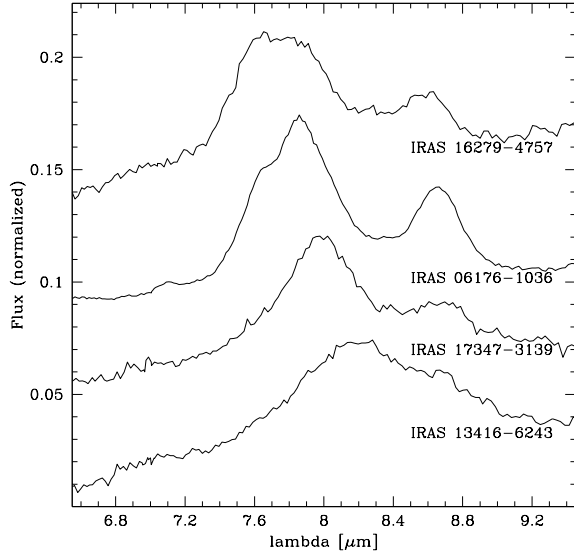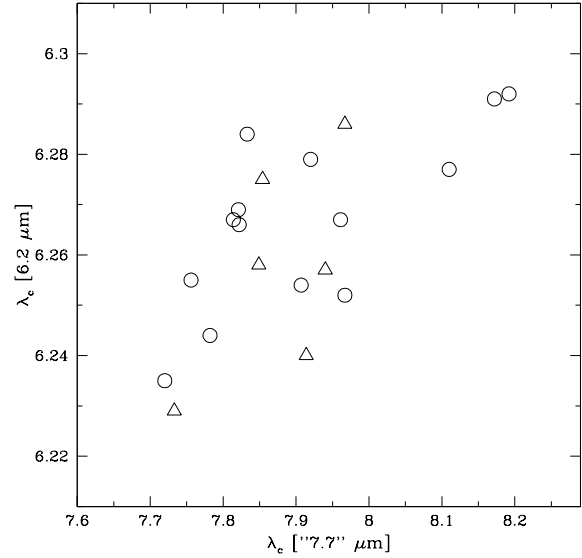
FIGURE 1. The normalized spectra of four post-AGB objects from our sample showing variations in the "7.7" μm peak shape and position.

FIGURE 2. Peak position of the "7.7" μm complex versus that of the 6.2 μm band. Open circles denote post-AGB objects and open triangles mark [WR] PNe.

(polynomial of order 1) and fitting a single Gaussian to the features at 3.3, 6.2, "7.7", 8.6 and 11.3 μm, separately. The "7.7" μm complex is treated similarly in spite of the evidence that (in many cases) this band is composed of at least two variable components (see Peeters et al. 2002 and references therein). In addition, we have used a single baseline underlying the "7.7" and 8.6 μm features, which passes through points from ~6-7 μm up to ~9-10 μm. Other ways of decomposing the UIR bands will yield slightly different results. However, these differences will affect all sources in a systematic way and the variations discussed here will remain.

We present in Table 1 our sample (IRAS name in column (2), galactic coordinates - column (3), the effective temperature, T_{eff} - column (4) - if available) and the obtained UIR band parameters (peak position, λ_c [μm], and the integrated fluxes of the Gaussian fits, F [W/cm^2]) for the 3.3, 6.2, "7.7", 8.6 and 11.3 μm features (columns (5), (6), (7), (8) and (9), respectively). The shapes of the band profiles will be discussed in the full version of the paper (Szczerba et al. in preparation).

DISCUSSION

The "7.7" μm band is composed of at least two sub-peaks and in some cases the main peak shifts up to 8 μm or more (see Peeters et al. 2002 and references therein). In Fig. 1 we show spectra of four post-AGB sources selected from our sample, which are ordered according

to the peak wavelength of the "7.7" μm complex. The whole range of possible peak shapes and positions are seen among post-AGB sources.

Peeters et al. (2002) and van Diedenhoven et al. (2004) classified objects, independently for each UIR band, into classes based on the band profile and peak position. They noted that the derived classes are directly linked with each other. Fig. 2 shows such a correlation between the "7.7" and 6.2 μm peak position for our sample of proto-PNe and PNe. In general, sources with a 6.2 μm feature peaking at longer wavelengths show also a "7.7" μm complex shifted toward the red. There is no sharp "jump" between their classes but rather a continuous transition in the peak position for both features It is possible that there is an abrupt "jump" to the band peaking at 8.1-8.2 μm. However, sources with the peak wavelength of the "7.7" complex shifted above 8 μm have a 6.2 μm band peaking at the longest wavelengths in accordance with the overall correlation seen in Fig. 2. Note, that there is no separation between post-AGB objects (circles) and [WR] PNe (triangles) on this diagram.

The peak of the 8.6 μm band remains well confined between 8.57 and 8.67 μm (with two exceptions) and does not show any correlation with the peak position of the "7.7" μm complex. Note, however, that there is no 8.6 μm band for objects which have "7.7" band peak shifted above ~8 μm. The two exception are: IRAS 22574+6609 (proto-PN no. 5 in Table 1.) with λ_c [8.6 μm] = 8.52 μm, and IRAS 04215+6000 ([WR] PN no. 7) with λ_c [8.6 μm] = 8.76 μm. In the latter case

TABLE 1. Central wavelengths and fluxes of UIR bands for sample of C–rich proto–planetary and [WR] planetary nebulae.

No	Object name	l	b	T_{eff} [K]	3.3 μm λ_c [μm] ; F [W/cm^2]	6.2 μm λ_c ; F	"7.7" μm λ_c ; F	8.6 μm λ_c ; F	11.3 μm λ_c ; F
(1)	(2)	(3)		(4)	(5)	(6)	(7)	(8)	(9)
proto-planetary nebulae:									
1	IRAS 19480+2504	061.84 −00.56						8.502 ; 7.684e-18	11.628 ; 3.626e-18
2	IRAS 20000+3239	069.68 +01.16		5500.	3.294 ; 3.098e-19	6.277 ; 1.065e-18	8.110 ; 1.272e-17		11.513 ; 4.321e-18
3	Egg Nebula	080.17 −06.50		6500.	3.293 ; 4.056e-19	6.291 ; 9.155e-18	8.172 ; 7.294e-17		11.357 ; 1.844e-17
4	IRAS 22272+5435	103.35 −02.52		5750.	3.275 ; 3.850e-19	6.252 ; 6.431e-18	7.967 ; 3.766e-17	8.631 ; 4.377e-18	11.346 ; 1.615e-17
5	IRAS 22574+6609	112.04 +05.96		5500.		6.254 ; 1.194e-18	7.907 ; 1.076e-17	8.517 ; 4.378e-18	11.379 ; 5.350e-18
6	IRAS 23304+6147	113.86 +00.59		6750.			7.963 ; 1.222e-17		11.371 ; 3.989e-18
7	IRAS 01005+7910	123.57 +16.59		21000.	3.277 ; 3.808e-19	6.228 ; 1.649e-18	7.565 ; 9.873e-18	8.625 ; 1.293e-18	11.258 ; 1.275e-18
8	IRAS Z02229+6208	133.73 +01.50		5500.		6.279 ; 5.352e-18	7.920 ; 1.625e-17	8.650 ; 6.917e-18	11.378 ; 1.365e-17
9	IRAS 04395+3601	166.45 −06.53		25000.	3.259 ; 5.649e-19				
10	IRAS 05341+0852	196.19 −12.14		6500.		6.284 ; 8.420e-19	7.833 ; 1.180e-17		11.333 ; 1.501e-18
11	IRAS 07134+1005	206.75 +09.99		7250.			7.766 ; 7.799e-18		11.316 ; 5.813e-18
12	IRAS 06176−1036	218.97 −11.76		7500.	3.294 ; 6.110e-17	6.267 ; 2.067e-16	7.814 ; 4.893e-16	8.665 ; 9.627e-17	11.264 ; 9.085e-17
13	IRAS 10158−2844	266.85 +22.93		7600.	3.293 ; 4.493e-18	6.269 ; 2.110e-17	7.821 ; 4.416e-17	8.659 ; 9.063e-18	11.272 ; 8.464e-18
14	IRAS 13416−6243	308.99 −00.73			3.295 ; 1.002e-18	6.292 ; 4.080e-18	8.192 ; 3.504e-17		11.417 ; 4.269e-18
15	IRAS 13428−6232	309.16 −00.59				6.255 ; 1.889e-18	7.756 ; 5.042e-18	8.625 ; 1.017e-18	11.305 ; 1.308e-18
16	IRAS 14316−3920	323.77 +19.10		6750.	3.293 ; 1.100e-18	6.301 ; 7.204e-18			11.339 ; 1.045e-18
17	IRAS 16279−4757	336.14 +00.09		4900.	3.288 ; 1.641e-18	6.235 ; 1.221e-17	7.720 ; 2.798e-17	8.595 ; 2.419e-18	11.265 ; 8.426e-18
18	IRAS 16594−4656	340.39 −03.29		12000.	3.289 ; 9.949e-19	6.244 ; 9.624e-18	7.782 ; 3.053e-17	8.580 ; 9.373e-18	11.271 ; 4.024e-18
19	IRAS 17311−4924	341.41 −09.04		21000.		6.266 ; 1.094e-18	7.822 ; 3.436e-18	8.629 ; 6.672e-19	11.280 ; 7.724e-19
20	IRAS 17347−3139	356.80 −00.06		15000.	3.295 ; 4.315e-19	6.267 ; 5.226e-18	7.961 ; 2.032e-17	8.653 ; 4.314e-18	11.409 ; 2.433e-18
[WR] planetary nebulae:									
1	IRAS 18129−3053	001.59 −06.72		35000.	3.290 ; 7.276e-19	6.275 ; 8.078e-18	7.854 ; 9.948e-18	8.658 ; 8.758e-19	11.215 ; 1.213e-18
2	IRAS 17262−2343	002.43 +05.85		151000.	3.305 ; 9.031e-19				11.317 ; 4.227e-18
3	IRAS 18240−0244	027.68 +04.26		65000.	3.292 ; 1.663e-18	6.257 ; 8.636e-18	7.940 ; 3.510e-17	8.631 ;1.072e-17	11.298 ; 4.524e-18
4	IRAS 19327+3024	064.79 +05.02		47000.	3.290 ; 5.960e-18		7.826 ; 1.054e-16	8.576 ; 3.865e-17	11.277 ; 2.967e-17
5	IRAS 20119+2924	068.35 −02.74		77000.	3.315 ; 5.472e-19			8.731 ; 2.482e-18	11.240 ; 2.540e-18
6	IRAS 00102+7214	120.02 +09.87		78000.	3.295 ; 3.046e-19		7.792 ; 3.043e-18	8.643 ; 9.087e-19	11.239 ; 9.369e-19
7	IRAS 04215+6000	146.79 +07.60		31000.		6.229 ; 3.572e-18	7.733 ; 8.990e-18	8.758 ; 2.035e-18	11.285 ; 1.197e-18
8	IRAS 07027−7934	291.38 −26.29			3.290 ; 1.554e-18	6.286 ; 1.419e-17	7.967 ; 4.634e-17	8.631 ; 1.074e-17	11.300 ; 9.212e-18
9	IRAS 13501−6616	309.11 −04.40			3.234 ; 8.292e-19				11.239 ; 3.841e-18
10	IRAS 14562−5406	321.05 +03.99		30000.	3.291 ; 6.416e-18	6.240 ; 4.086e-17	7.914 ; 1.351e-16	8.589 ; 4.295e-17	11.293 ; 1.928e-17
11	IRAS 15559−5546	327.19 −02.20			3.288 ; 1.007e-18		7.781 ; 1.887e-17	8.633 ; 5.031e-18	11.254 ; 4.415e-18
12	IRAS 17047−5650	332.92 −09.91		32000.	3.290 ; 7.368e-18	6.258 ; 4.816e-17	7.849 ; 1.919e-16	8.587 ; 4.499e-17	11.298 ; 3.127e-17
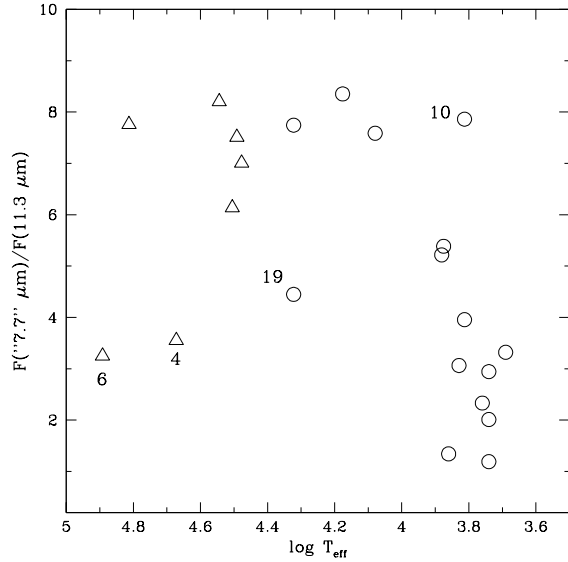
FIGURE 3. Flux ratio of the "7.7" μm complex and the 11.3 μm band. Meaning of symbols is the same as in Fig. 2. Numbers from Table 1 identify objects for which position on the diagram deviates from the general trend.

the peak position is uncertain due to low S/N of the ISO spectrum.

The peak of the 3.3 μm band is even more confined. It is located between 3.287 and 3.296 μm with the exception of two post-AGB objects: IRAS 22272+5435 (no. 4) which have λ_c [3.3 μm] = 3.275 μm, and IRAS 01005+7910 (no. 7) with λ_c [3.3 μm] = 3.277 μm. On the other hand, the peak position of the 11.3 μm band is not so "stable" ($\Delta\lambda_c$ [11.3 μm] $\approx$0.2 μm). Note that λ_c [11.3 μm] correlates with the "7.7" μm band peak in a similar way as shown in Fig.2.

The "7.7" μm complex (if present) is one of the strongest among the UIR bands. Its strength depends critically on the ionization state of the emitting PAH molecules (see discussion in Peeters et al. 2002). During evolution from AGB to PNe the stellar effective temperature increases steadily and we can expect that PAH molecules formed on the AGB will become ionized and the "7.7" μm to 11.3 μm flux ratio (which decreases after ionization of the PAH molecules) will become higher. Fig. 3 shows this flux ratio as a function of the stellar effective temperature. If one discards [WR] PNe no. 4 and 6 and proto-PN no.19, the general tendency is an increase of this flux ratio with increase of T_{eff}, levelling off at about log(T_{eff})$\sim$4.2. The exceptions are: post-AGB object no.19 - IRAS 17311$-$4924 and [WR] PNe no.4 - IRAS 19327+3024 and no.6 - IRAS 00102+7214. These exceptions can not be rather explained by the uncertainties in their spectra. It seems also that IRAS 05341+0852

(no.10) has slightly too high F("7.7" μm)/F(11.3 μm) for so low stellar temperature.

CONCLUSIONS

By investigation of UIR band features in 20 post-AGB objects and 12 [WR] PNe (a sample more limited from a physical point of view than the sample analysed by Peeters et al. 2002 and van Diedenhoven et al. 2004 which includes star forming regions, H II regions, Herbig Ae Be stars, galaxies as well as proto-PNe and PNe) we have shown that there are clear variations in the UIR bands parameters resulting (possibly) from PAH modification (chemical or/and physical) due to the circumstellar shell and/or star evolution. We have shown the existence of a correlation between UIR band flux ratios and the star's temperature. Possibly the ionization of the UIR band carriers is responsible for variation of F("7.7" μm)/F(11.3 μm) with the hardening of the radiation field. Such a conclusion could be reached because the effective temperature can be determined for proto-PNe and PNe. In the heterogenous sample of Peeters et al. (2002) there is no easy way to determine the physical parameters in a consistent manner.

REFERENCES

Boersma, C., Hony, S., & Tielens A.G.G.M. 2005, A&A, in press

Cohen, M., Barlow, M.J., Sylwester, R.J., et al. 1999, ApJ, 513, L135

de Graauw, T., Haser, L.N., Beintema, D.A., et al. 1996, A&A, 315, L49

Kessler, M.F., Steinz, J.A., Anderegg, M.E., et al. 1996, A&A, 315, L27

Li, A. 2004, in Astrophysics of Dust, ed. A.N. Witt, G.C. Clayton and B.T. Draine, ASP Conference Series, 309, 417

Peeters, E., Hony, S., Van Kerckhoven, C., et al. 2002, A&A, 390, 1089

Siódmiak, A. 2005, PhD thesis, N. Copernicus Astronomical Center

Szczerba, R., Górny, S.K., Stasińska, G, et al. 2001, A&SpS, 275, 113

van Diedenhoven, B., Peeters, E., Van Kerckhoven, et al. 2004, ApJ, 611, 928

Waters, L.B.F.M., Beintema, D.A., Zijlstra, A.A., et al. 1988, A&A, 331, L61